*ENGINEERING TRANSACTIONS* • *Engng. Trans.* **46**, 3–4, 291–314, 1998
Polish Academy of Sciences • Institute of Fundamental Technological Research
10.24423/engtrans.646.1998

# MECHANICAL CHARACTERIZATION OF THE INTERFACE BETWEEN A SHAPE MEMORY ALLOY FIBER AND A RESIN EPOXY MATRIX

F. THIEBAUD, B. GABRY
and C. LEXCELLENT (BESANÇON)

The aim of this paper is to characterize the interface between a shape memory alloy wire (SMA) and a epoxy resin matrix. Here we present the effect of various surface treatments applied to SMA NiTi wires on the quality of the interface fiber/matrix. First, the use of the fiber pull-out test allows to separate the different treatments into two families: on the one hand, decohesion of the wire; on the other hand, rupture of the wire before debonding. The data given by the pull-out tests are not sufficient to differenciate the surface treatments which cause the breaking of the wire rather than the interfacial debonding of the fiber/matrix. In order to complete our research, a topographical study is carried out on different wires. It allows us to extract the parameters which characterize the vertical distribution of roughness and its morphology. The analysis of these experimental results leads to the choice of the surface treatment which will guarantee higher interfacial stresses. Among all the wires studied, we choose the prestrained wire. The quantitative aspect of this study allows us to know better the evolution of the different parameters of roughness, and thus to guide our research works to an optimal surface treatment of the wire.

Key words: Shape memory alloy, composite material, interface fiber-matrix, pull-out test, surface treatments, roughness, smart material.

## NOTATIONS

| | |
|---|---|
| $A_s^0$ | Austenite initial temperature at free stress state |
| $A_f^0$ | Austenite final temperature at free stress state |
| $M_s^0$ | Martensite initial temperature at free stress state |
| $M_f^0$ | Martensite final temperature at free stress state |
| $F_d$ | debonding force measured during the pull-out test |
| $F_r$ | fracture force of the wire |
| $\tau_{\max}$ | shear stress induced by the debonding force |

*Parameters for characterizing the amplitude property (amplitude parameters)*

| | |
|---|---|
| SRa | dispersion parameter defined as the arithmetic mean of the absolute values of the surface displacements above and below the mean plane within the sampling area |
| Rtm | maximum value of the summit to valley height in the sampling area |
| Rpm | lowest value of the valley in the sampling area |

| | |
|---|---|
| Rvm | highest value of the summit in the sampling area |
| SRku | measure of the sharpness of the surface height distribution |
| SRsk | measure of the asymmetry of surface deviations about the mean plane |

*Parameters from Abbott-Firestone curve*

| | |
|---|---|
| Rk | the core roughness depth measures the height of the core material portion |
| Rpk | the reduced peak height beyond the core profile |
| Rvk | the reduced valley depth below the core profile |
| MR1 | denotes the bearing area points of Rpk |
| MR2 | denotes the bearing area points of Rvk |
| Kp | coefficient of hollowness |

## 1. INTRODUCTION

In the field of composite materials, the shape memory alloys (SMA) actuators have recently attracted interest. Compared with more classical materials, SMA present a lot of efficient thermomechanical properties : very large recovery strain ($> 5\%$) and the ability to generate large stresses ($> 400$ MPa) by simple heating. The unique properties of SMA are on the one hand related to a displacing, diffusionless and recoverable phase transformation (superelasticity, recovery stress...), and on the other hand, a reorientation process of the martensite phase (one way shape memory effect, damping...). Hence, the martensite phase obtained under cooling at free stress state is characterized by a fine network structure of self-accommodating platelets which can be re-oriented by applying an external stress action. The domain with a favorable orientation towards the direction of the applied stress produces a strain which gives a macroscopic deformation of the material. This deformation is totally recovered by heating the sample at the characteristic austenite final temperature ($A_f^0$). But if the shape recovery is prevented by a clamping device or if the SMA wire is embedded in a epoxy resin matrix, a stress will be generated and it is referred to as recovery stress.

Hence, layers of SMA fibers can be embedded in composites and used to active control, e.g. sample geometrical shape, stiffness and in consequence, natural frequencies of vibration [1, 2, 3]. Numerous experimental researches have been devoted to these new materials; the interaction between SMA and the matrix, and the effect of the matrix on the phase transformation of the fiber have been studied [4, 5]. Models describing SMA matrix interaction and predicting thermomechanical behavior have been developed [6, 7]. In order to elaborate smart composite structure, the study of the quality of the interface SMA/matrix is crucial. The transfer of the SMA recovery strain (one-way shape memory effect) in a soft matrix or of the SMA recovery stress in a stiff matrix must be efficient. Interface decohesion or sliding must be avoided. In this paper, the effects of sur-

face treatment of the SMA wire (sanding, anodisation, predeformation....) on the quality of the interface are examined. Thus, two tools are chosen: the pullout test in order to evaluate the adhesion strength between the SMAand the matrix, and the profilometry – to determine the geometrical shape of the SMA wire surface.

## 2. Material and techniques

The pull-out tests are performed on an epoxy circular sample containing one embedded NiTi wire placed at the center. The fiber is of 200 μm diameter NiTi SMA (50,2 at % Ni) supplied by the Furukawa society. The resin, supplied by the Ciba-Geigy company is composed of LY556 bisphenol epoxy resin, HY 917 anhydride hardener and DY070 amino accelerator, mixed in the proportions 100/90/0,5 by mass. The resin was cured for two hours at 80 °C, then cured for four hours at 140 °C.

Modelling of the viscoelastic behavior of the resin and the thermomechanical response of the NiTi S.M.A. in the space $\{\sigma, \varepsilon, T\}$ has been performed [8, 9]. In order to improve the effect of the S.M.A. surface state on the quality of the adhesion, the following treatments have been done on the fibers.

### *2.1. Unrefined wire cleaned by ultrasonics*

After wire drawing, the wire is annealed for twenty minutes at 400 °C and air – cooled. The aim of this treatment is to stabilize the austenitic phase at ambient temperature, more precisely the rhombohedrical phase (Rphase: e.g. Fig. 1). The wire is then thoroughly rinsed in an acetone solution subjected to ultrasonics in order to remove grease and other impurities.

### *2.2. Wire glass – blasted*

The unrefined wire is subjected to a bombing of glass micromarbles for two minutes.

### *2.3. Wire anodized*

This operation, so-called anodization, consists in immersing the wire in a sulfuric acid solution (concentration: 200 g/l) at ambient temperature. A generator of current, bound at a platinum electrode and the wire (cathode), delivers an intensity of $2\text{A/dm}^2$. It allows us to obtain variable oxide film thickness which

depends on the voltage applied and the length of the anodization. In our case, we fix this last parameter at twenty minutes [10].

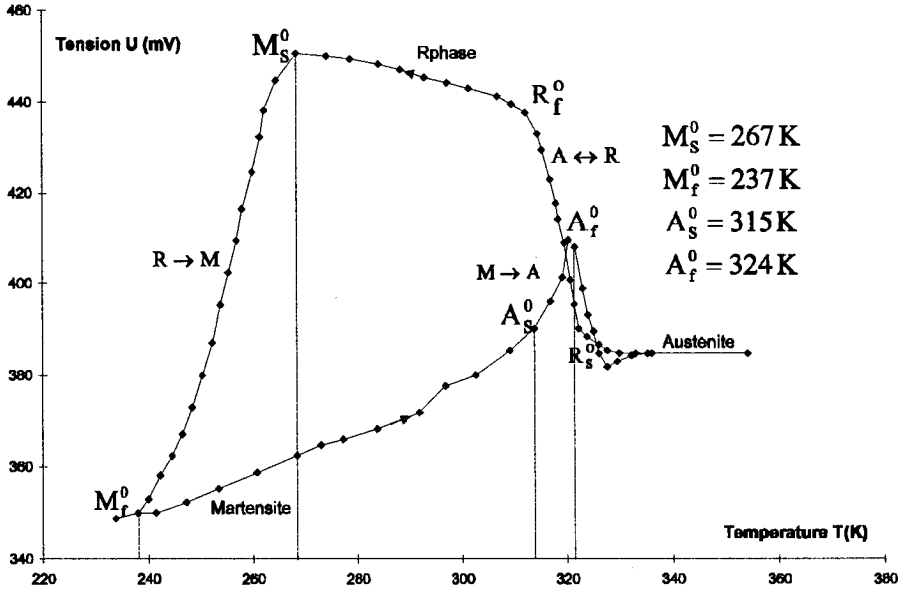


FIG. 1. Electrical resistivity at free stress state.

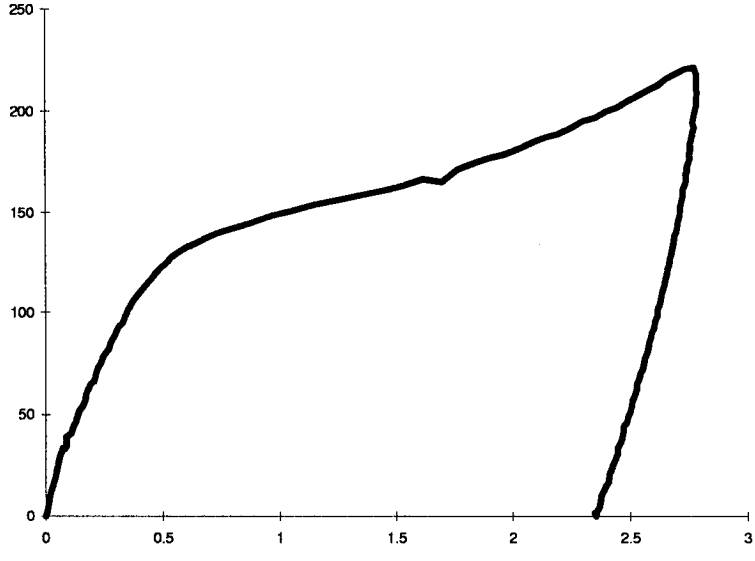


FIG. 2. Loading-unloading tensile test at $T = 24$ °C.

### *2.4. Prestrained wire*

A loading-unloading tensile test is carried out on the unrefined wire at ambient temperature. It causes the phase transformation Rphase $\rightarrow$ stress-induced martensite, and after unloading, it subsists a residual deformation (residual strain $= 2.35\%$) called pseudoplastic one.

### *2.5. Prestrained glass-blasted and prestrained anodised wires*

These categories of wires are the result of combination of the treatments used previously.

## 3. Characterization of the interface fiber/matrix

First of all, it is important to choose a test which will allow us to obtain a physical scale of the interfacial adhesion of the SMA wire to a polymer matrix. Indeed, understanding the interaction between the embedded fiber and the host material is crucial to design a reliable, smart structure. Several tests, like pull-out tests [11] or fragmentation techniques [12] have been applied to measure the fiber/matrix adhesion. But this last test cannot be applied to our structure because one of the components doesn't support a fracture strain much larger than the other one (at least 4 times). In our case, we have $(\varepsilon_r)_{\text{matrice}} = 4\%$ to $7\%$ and $(\varepsilon_r)_{\text{fil}} = 10\%$ to $15\%$. Therefore, only the shrinking test can be used.

### *3.1. Pull-out test*

**Principle**: it consists in pulling-out a single filament embedded in a host material by one length. Four tests are realized for each type of wires. These tests are performed in an Instron machine using a constant speed of 0.5 mm/sec. A diagram of a typical pull-out test (load-time) is shown in Fig. 3. Debonding is characterized by a sudden drop in the load applied to the wire. The maximal value of the load is referred to the debonding force.

**Theoretical analysis**: a simplified approach consists in supposing that the shear stress induced at the SMA. Host interface is constant along the fiber. We have:

$$\tau = \frac{F_d}{S} = \frac{F_d}{2\pi r L} \tag{3.1}$$

$F_d$ is the debonding force (determined experimentally), $r$ – radius of the fiber, $L$ – embedded length.

This first approach being a little too simple, we use GRESZCZUK'S modelling [13] which gives the analytical formulation of the distribution of the shear stress along the fiber. In this case, this stress is no more supposed to be constant. The evolution of this shear stress versus the embedded length is represented in Fig. 4:

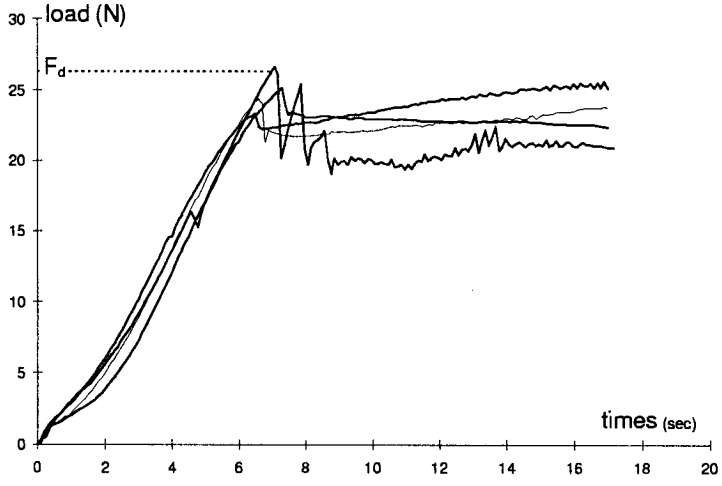


FIG. 3. Experimental pull-out curves for 4 different unrefined wires.

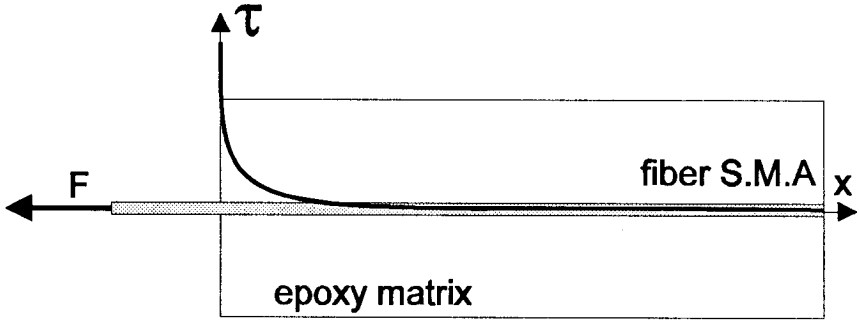


FIG. 4. Evolution of the shear stress induced in the material.

The expression of this stress is given by the relation:

$$\tau(x) = F_d \frac{\alpha}{2\pi r} [\mathrm{cth}(\alpha \cdot L)\mathrm{ch}(\alpha \cdot x) - \mathrm{sh}(\alpha \cdot x)] ,$$

(3.2)

$$\alpha = \sqrt{\left| 2\pi \frac{G_m}{\ln\left(\frac{r}{R}\right)} \left( \frac{1}{\pi r^2 E_f} - \frac{1}{\pi R^2 E_m} \right) \right|} .$$

$G_m$ – shear modulus of the matrix, $E_m$ – Young's modulus of the matrix, $E_f$ – Young's modulus of the fiber, $r$ – radius of the fiber, $R$ – radius of the host material, $L$ – embedded wire length.

REMARKS

(a) We observe that $\tau$ is maximum for $x = 0$ and is given by

$$\tau_{\max} = \tau(x = 0) = F_d \frac{\alpha}{2\pi r} \operatorname{cth}(\alpha \cdot L), \qquad F_d = F_r. \tag{3.3}$$

(b) We have two values of $E_f$ depending on whether the wire is in a martensitic state or in a rhombohedrical phase, so-called Rphase.

### *3.2. Sample geometry*

The choice of the length of the samples depends on the rupture strength in tension of $F_r$ the SMA wires. Indeed, we must imperatively obtain the debonding fiber/matrix before the wire breaks. We must have $F_d$ below $F_r$. Rupture tests in tension show that, independently of the initial the crystalline state of the wire, we have only one rupture strength. From the experimental results, we measure $F_r = 37,4$ N. This result explains oneself by the fact that all the wires are, just before rupture, in martensitic phase [14].

The next curve (Fig. 5) presents the theoretical interfacial stress, reaching maximum for $x = 0$, versus the length of the sample

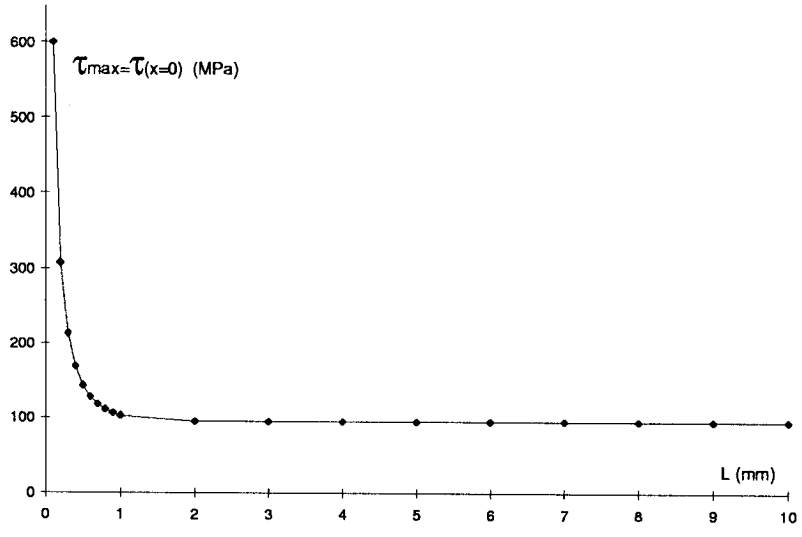


FIG. 5. Evolution of the maximum interfacial stress $\tau_{\max} = \tau(x = 0)$ with the length of the sample.

We remark that for a length $L < 3$ mm, $\tau_{\max}$ increases. If we want to obtain the decohesion fiber/matrix before the wire breaks, we should choose a length which gives the largest possible shear stress, so $L < 3$ mm. Meanwhile, for experimental reasons, we can not realize such specimens, and finally we prepare circular specimens of outer diameter 13 mm and the embedding is chosen as 20 mm. For this type of specimens, the theorical maximum shear stress that we can reach is $\tau_{\max} = 94$ MPa.

### *3.3. Results of analysis*

In order to compare the pull-out tests carried out on the wires, we calculate the value of the interfacial maximum shear stress after Greszczuk from the value of the debonding force measured. The mean pull-out force for each type of wires is listed in Table 1, this force being considered as an indicator of bond strength.

**Table 1. Pull-out tests results.**

| State of the wire | Initial crystallographic structure | $F_d$ measured (N) | Standard deviation | $\tau_{\max}$ (MPa) | Observations |
|---|---|---|---|---|---|
| cleaned (ultrasonics) | Rphase | 24.8 | 1.1 | 62.5 | Debonding |
| blasted (glass) | Rphase | 23.3 | 0.9 | 58.7 | Debonding |
| anodized (20 mn) | Rphase | 33.9 | 2.0 | 85.5 | *rupture of wire* |
| prestrained | Martensite+Rphase | 31.1 | 2.7 | 78.4 | *rupture of wire* |
| prestrained blasted | Martensite+Rphase | 31.6 | 2.6 | 79.7 | *rupture of wire* |
| prestrained anodized | Martensite+Rphase | 30.8 | 2.3 | 77.6 | *rupture of wire* |

$E_f$ martensite $= 24000$ MPa, $G_m = 1259$ MPa, $r = 0.1$ mm, $R = 6.5$ mm,
$E_f$ Rphase $= 31000$ MPa, $E_m = 3400$ MPa, $L = 20$ mm

Two types of results follow from this table: on the one hand, the debonding fiber/matrix and, on the other hand, rupture of the wire in tension. Moreover, the glass blasting brings nothing in comparison with the unrefined wire. We can make the hypothesis that the micromarbles of glass are not resistant enough compared with the nickel-titanium. As regards the other treatments, the length chosen doesn't allow to reach a sufficient interfacial stress to pull-out the wire. When there is rupture of the wire, we cannot conclude anything about the effects of the different surface treatments, we can just say that they improve the adhesion at the fiber/matrix interface. In order to characterize the better treatment

among all, we continue this work by studying the external surface of the wire. Indeed, observations made by SEM show important alterations of the aspect of the external envelope of the wire.

## 4. Profilometric analysis

In order to complete the works concerning the pull-out, we perform the topographical study of each wire. The most common technique to assess the surface characteristics is through the use of a stylus-based measurement for a predetermined distance and circumference. The geometry of the diamond mounted on the end tip is characterized by a conical shape: angle at the top of tip 90° and a rounded shape: radius of the tip sphere 5 $\mu$m. Owing to the small size of the wire (0.2 mm), a perfect manipulation is very important because the measurements can lead to dispersed values. In the case of a cylindrical surface, a certain number of parallel profiles must be collected. In the case of our measurements, the experimental assembly doesn't allow us to measure all the cylindrical surface but only 225°, and two lengths are chosen (5 mm and 0.39 mm).

After data acquisition, we obtain a cartography of the roughness of the wires. From this original surface, in order to separate roughness, waveness and form, some 2D digital filters are employed. As the first filtering is applied, we obtain a fitted polynomial surface which characterizes the form error which is the overall deviation of the real surface from the geometrical one. But in our case, because of the low values of roughness, a second filtering was necessary in order to separate parasitic phenomena like sound, machine tool vibration from the real roughness. In the next figures we present these different operations of filtering in the case of the anodised wire.

In order to observe rapidly the consequences of the surface treatments on the external surface, the software allows us to obtain a 3D image of the surface measured from the working surface, all the surfaces having the same scale following the $Z$ axis (between 0 and 3,5 $\mu$m).

The three-dimensional view of the glass-blasted surface shows that it is not very much different from the unrefined one, and seems to confirm the observations obtained by MEB. Moreover, the surface of the prestrained wire is more broken than the unrefined wire. The predeformation causes some defaults which have a periodic distribution (waves) on the circumference of the wire. So, we can notice that a simple tensile test generating a 2.35% residual strain modifies considerably its external surface. All these differences are observed too from the photos obtained with the MEB.

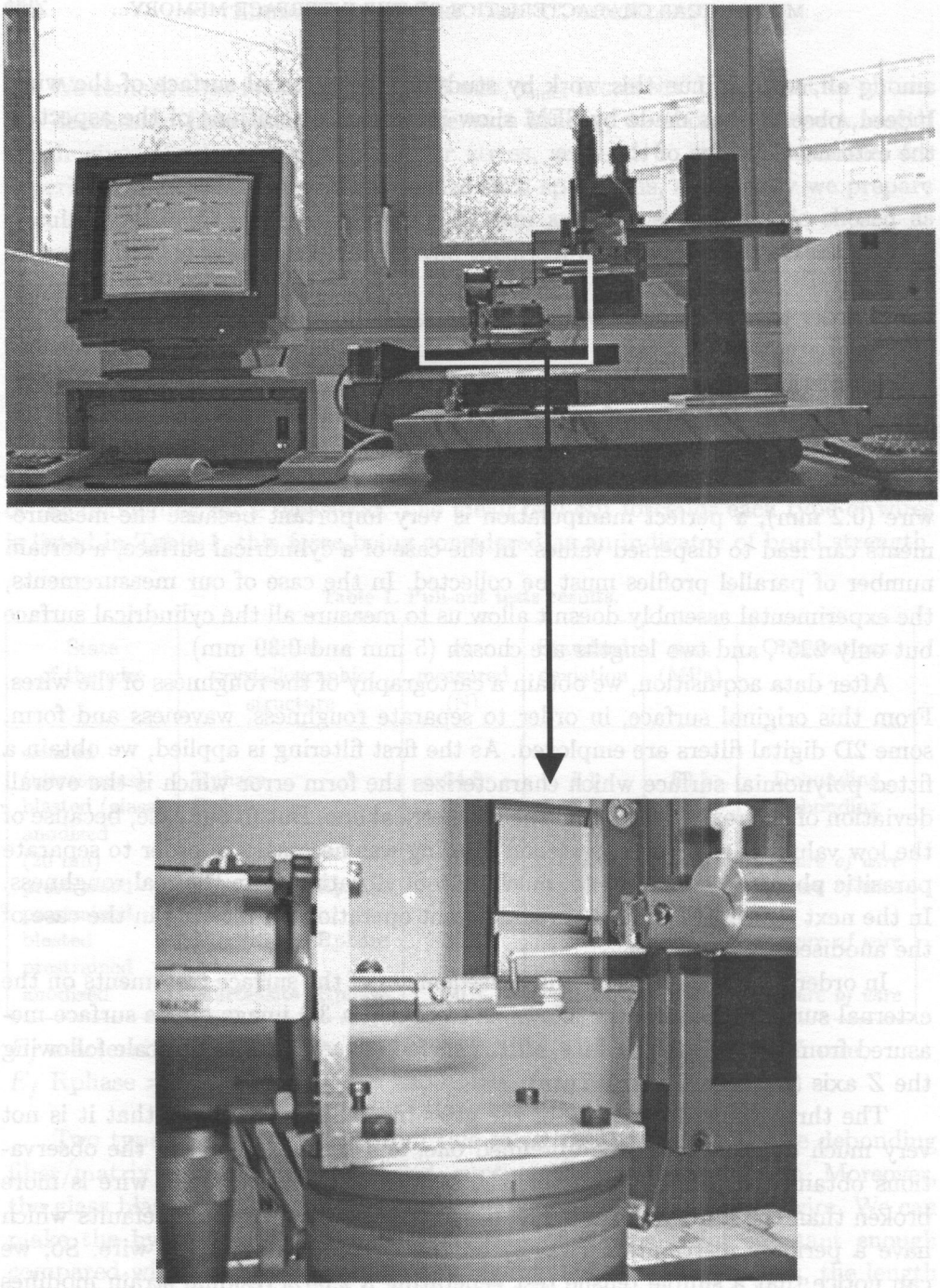

FIG. 6. Experimental set-up: data acquisition and $X$-$Y$-$Z$ system with the surface to be analyzed under the sensor.

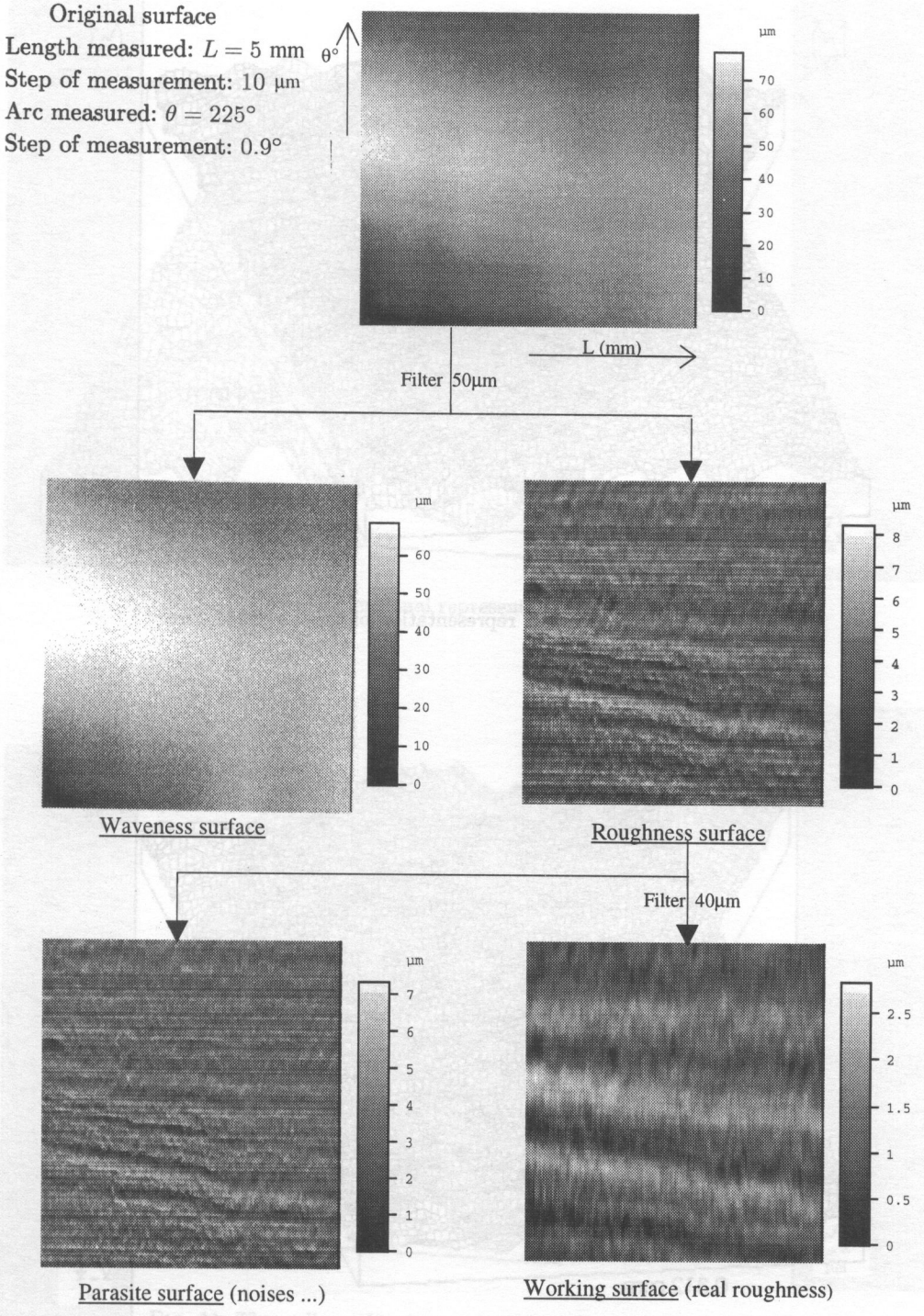


FIG. 7. Set of analysis operations (anodized wire).

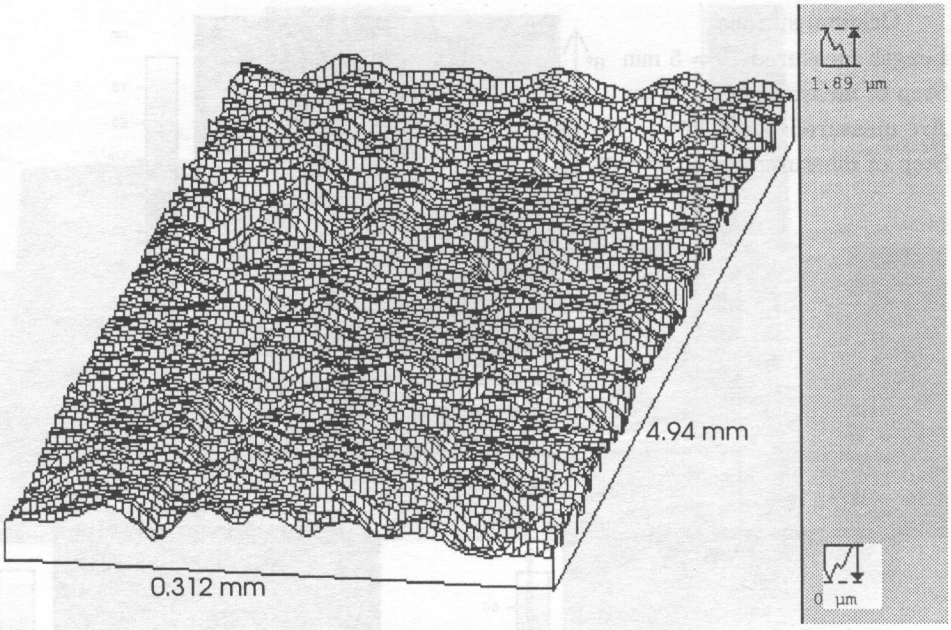


FIG. 8. Three-dimensional representation of the unrefined wire.

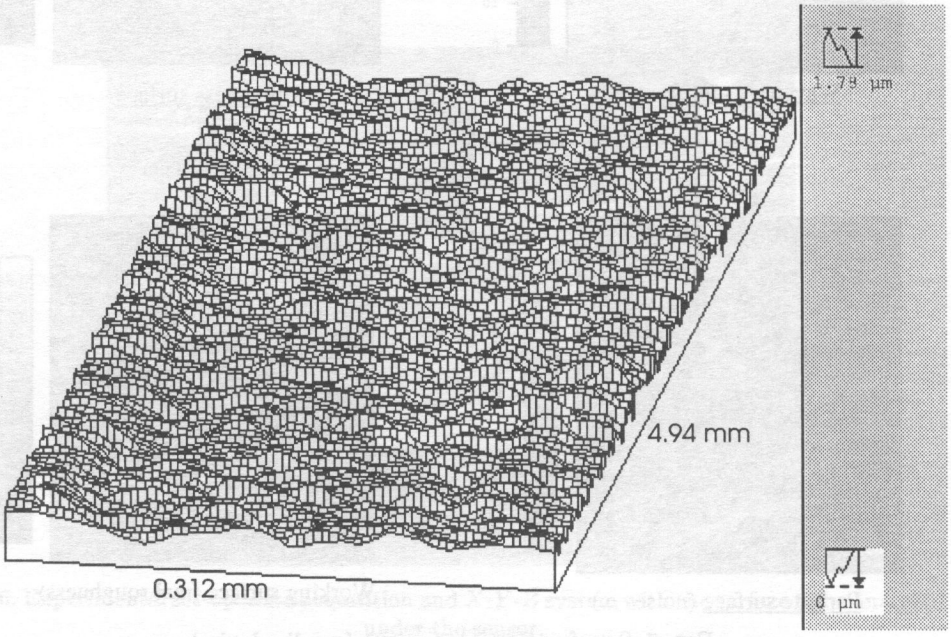


FIG. 9. Three-dimensional representation of the glass-blasted wire.

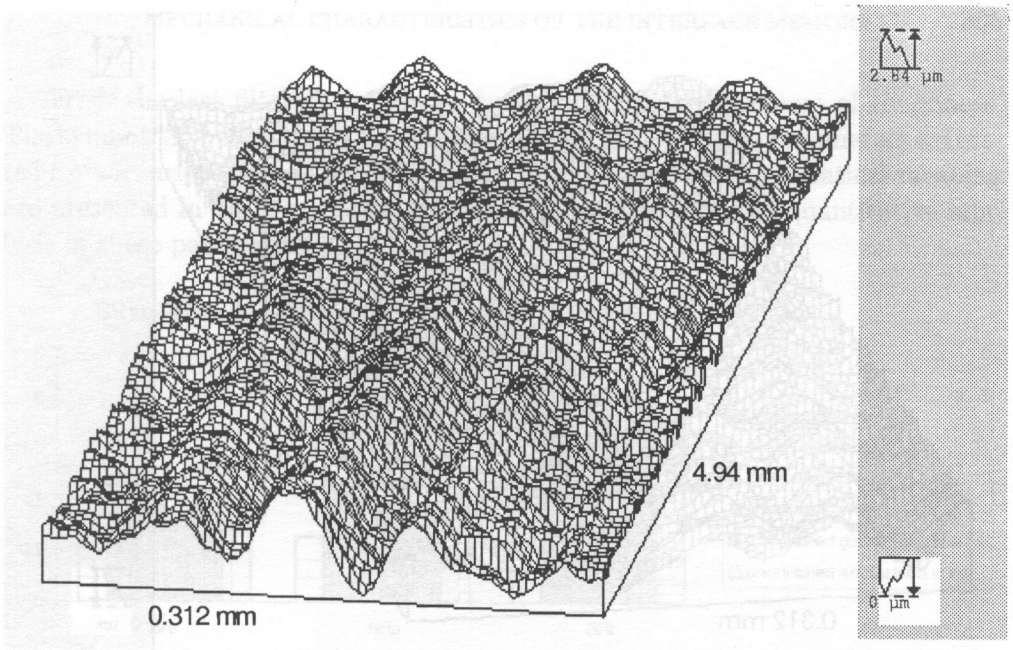


FIG. 10. Three-dimensional representation of the anodized wire.

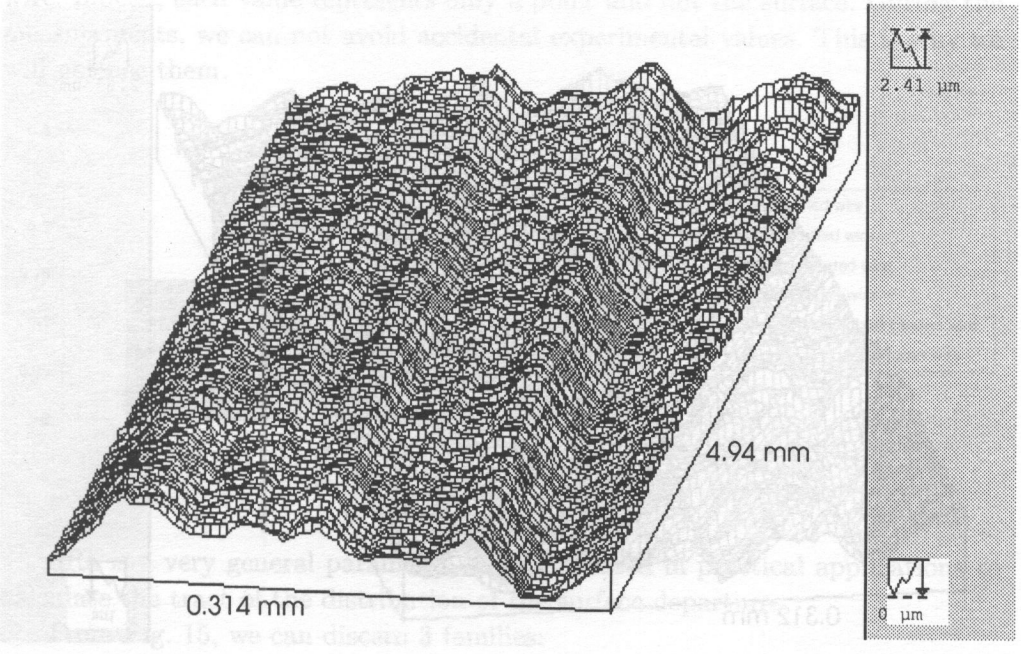


FIG. 11. Three-dimensional representation of the prestrained wire.

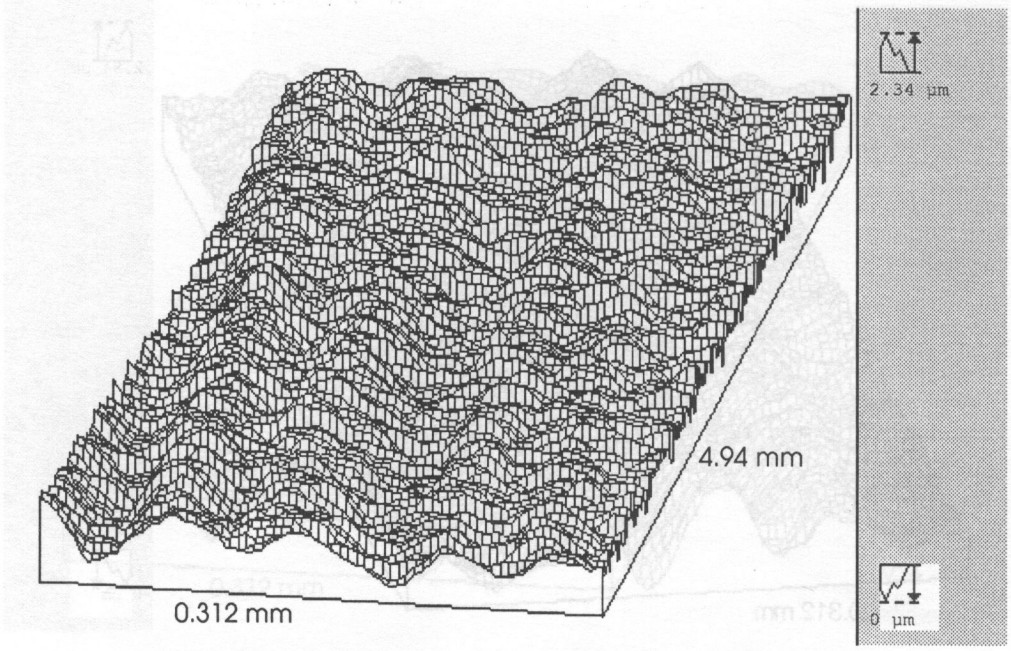


FIG. 12. Three-dimensional representation of the prestrained glass-blasted wire.

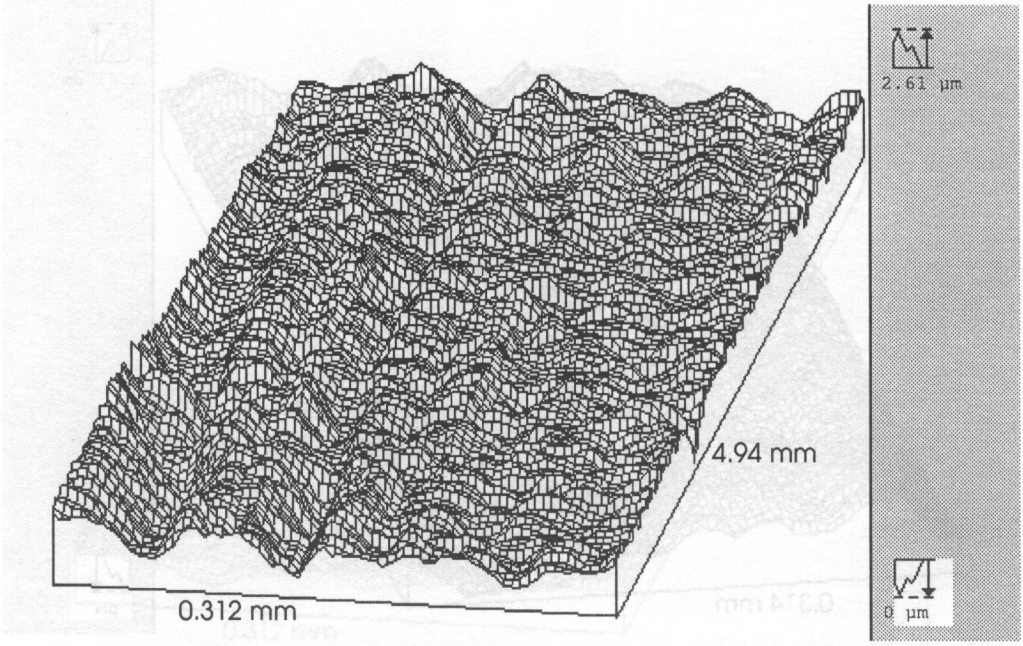


FIG. 13. Three-dimensional representation of the prestrained anodised wire.

From the last filtered surface we extract different parameters of roughness. The symbol "S" before these parameters signifies that they are parameters extracted from a surface and not from a profile. Their respective mathematical meaning are presented in the Appendix. The next graphics present the quantitative analysis of these parameters.

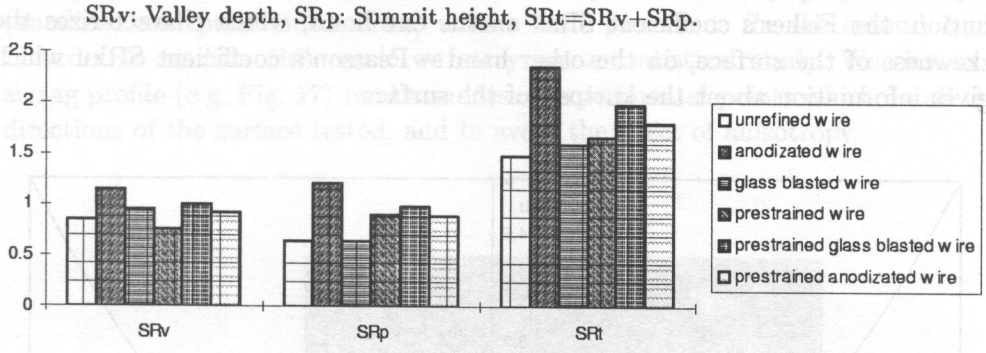


FIG. 14. Roughness parameters.

These 3 parameters are not sufficiently representative of the roughness of the wire. Indeed, each value represents only a point and not the surface. During the measurements, we can not avoid accidental experimental values. This is why we will not use them.

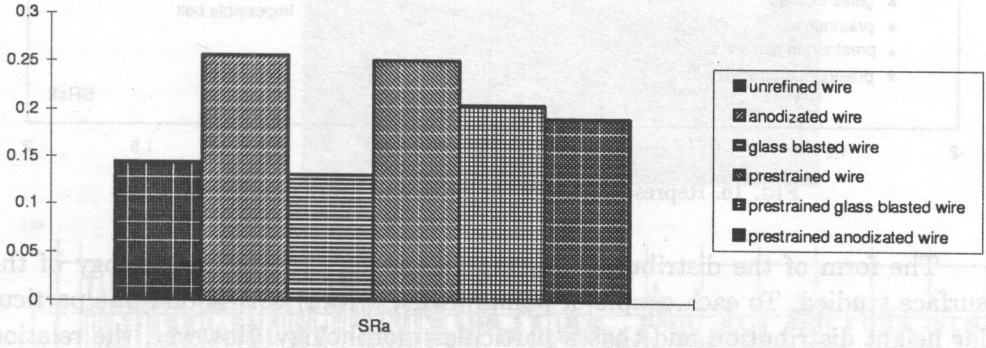


FIG. 15. Roughness parameter SRa.

SRa is a very general parameter commonly used in practical applications to calculate the tract of the distribution of the surface departures.

From Fig. 15, we can discern 3 families:

– unrefined wire and glass-blasted wire (SRa = 0.135 μm),

– prestrained glass-blasted and prestrained anodized wires (SRa = 0.195 μm),

– anodized wire and prestrained one (SRa = 0.255 μm).

By analogy with the results of the pull-out tests, it seems that for a SRa value increasing we would have a better fiber-matrix adhesion. However, SRa is a parameter which gives information about the amplitude of the defaults but not about the form. Indeed, for the same value of SRa we can have completely different surfaces.

Two other parameters are used to characterize the form of the height distribution: the Fisher's coefficient SRsk on the one hand, which characterizes the skewness of the surface, on the other hand – Pearson's coefficient SRku which gives information about the kurtosis of the surface.

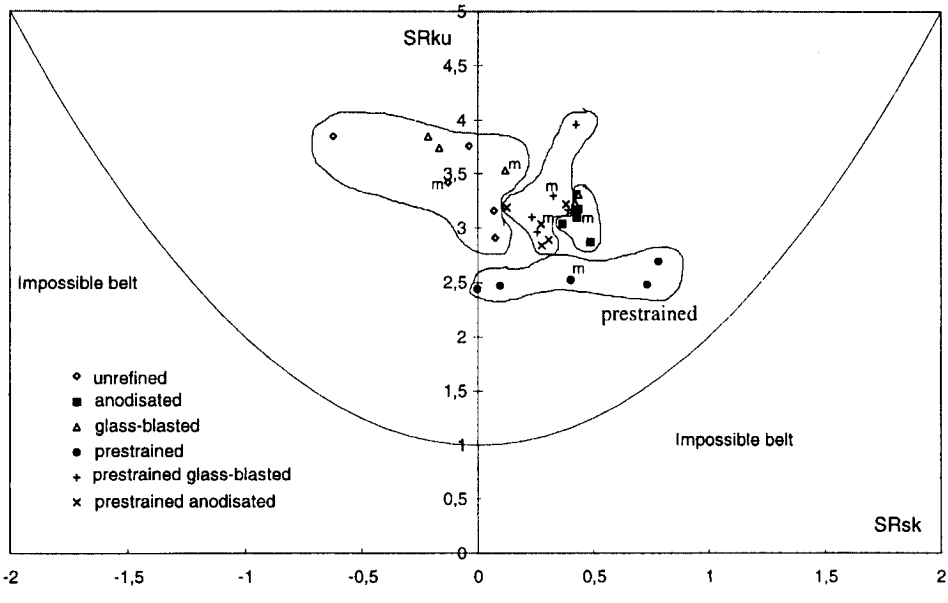


FIG. 16. Representation of the SRsk and SRku coefficients.

The form of the distribution corresponds in fact to the morphology of the surface studied. To each couple of points (SRsk, SRku) correspond one particular height distribution and thus a particular morphology. However, the relation existing between the profile and the height distribution is not a bijective function: several profiles can have the same height distribution.

Due to the fact that these values present some dispersions, we plot in the plane (SRsk, SRku) all these values of these couples as the average for each type of wires (symbol $m$).

*A priori* it seems to be difficult to draw any conclusions from this curve. But we remark that in the left superior zone of this graph the wires which gave the worse loading transfers. They are opposed to the prestrained wires. So we

can conclude that the morphology desired is characterized by a SRsk $\geqslant 0$ and SRku $< 3$.

An increase of SRsk means an asymmetric distribution which has a long tail in the maximum value side, and Srku$< 3$ gives a distribution with a shape of smoother peak, in this case the valleys and the peaks are removed from the average plane. Two types of wires are not subject to this topographic analysis (anodized and prestrained wires) with a little preference for the second ones. In order to confirm this result we carry out a statistical study. We choose a zigzag profile (e.g. Fig. 17) to obtain lots of experimental points which do all the directions of the surface tested, and to avoid the effect of anisotropy.

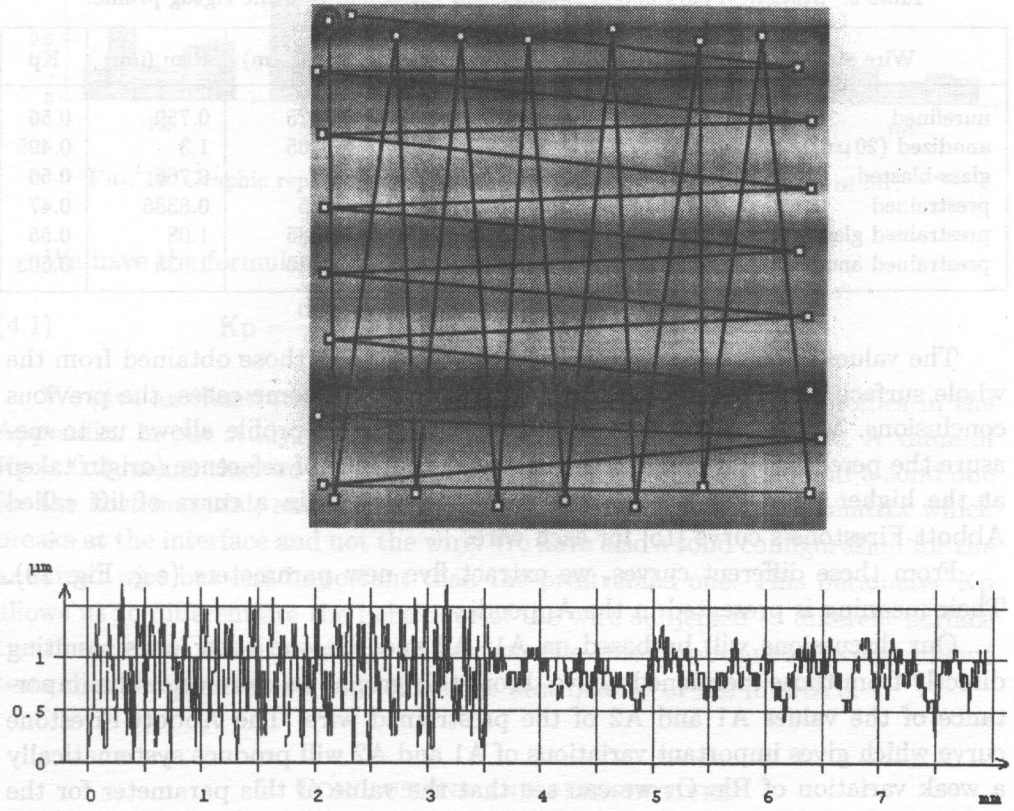


FIG. 17. Schematic representation of the zigzag profile choosen and its developed form.

From this profile, different normalized parameters are determined, including Rpm, Rtm, and Kp defined in the Appendix.

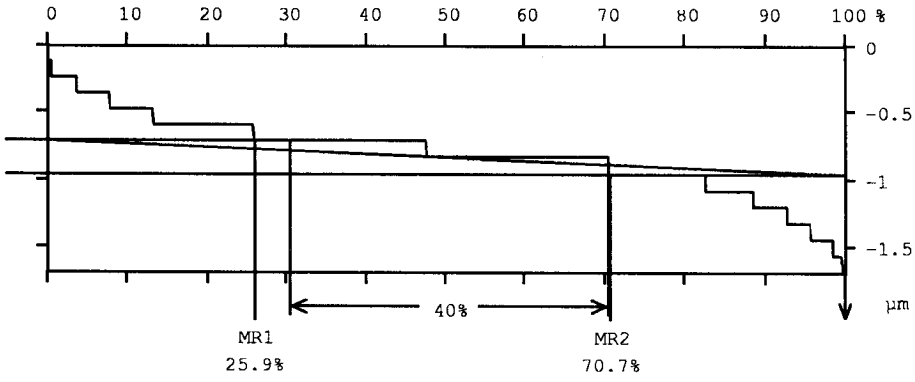


FIG. 18. Abbott-Firestone's curve of a prestrained wire.

**Table 2. Statistical parameters of roughness extracted from the zigzag profile.**

| Wire state | Ra ((µm) | Rsk | Rku | Rpm (µm) | Rtm (µm) | Kp |
|---|---|---|---|---|---|---|
| unrefined | 0.133 | −0.2425 | 3.86 | 0.3375 | 0.759 | 0.56 |
| anodized (20 µn) | 0.24 | 0.10995 | 3.265 | 0.6565 | 1.3 | 0.495 |
| glass-blasted | 0.122 | −0.3575 | 3.95 | 0.34 | 0.768 | 0.56 |
| prestrained | 0.1615 | 0.0452 | 2.74 | 0.445 | 0.8385 | 0.47 |
| prestrained glass-blasted | 0.171 | −0.21673 | 3.93 | 0.4885 | 1.08 | 0.55 |
| prestrained anodized | 0.173 | 0.0061 | 3.21 | 0.5145 | 1.035 | 0.503 |

The values of these parameters are less precise than those obtained from the whole surface, but they allow us to validate, except in some cases, the previous conclusions. Moreover, the numerical treatment of this profile allows us to measure the percentage of points located between a value of reference (origin taken at the higher point) and a depth of any cut. We obtain a curve of lift called Abbott-Firestone's curve [15] for each wire.

From these different curves, we extract five new parameters (e.g. Fig. 19). Their meaning is presented in the Appendix.

Our discussions will be based on A1, A2 and Rk, the other ones resulting directly from those mentioned above. From this graph, we can notice the importance of the values A1 and A2 of the prestrained wire. The Abbott-Firestone curve which gives important variations of A1 and A2 will produce systematically a weak variation of Rk. Or we can see that the value of this parameter for the prestrained wire is more meaning than that of the anodized wire. According to the lower value of the parameter Rk, the prestrained wire appears again to be the optimal solution for the loading transfer.

Another parameter is used as well to obtain information on the form of the height distribution: it is the coefficient of hollowness [16]:

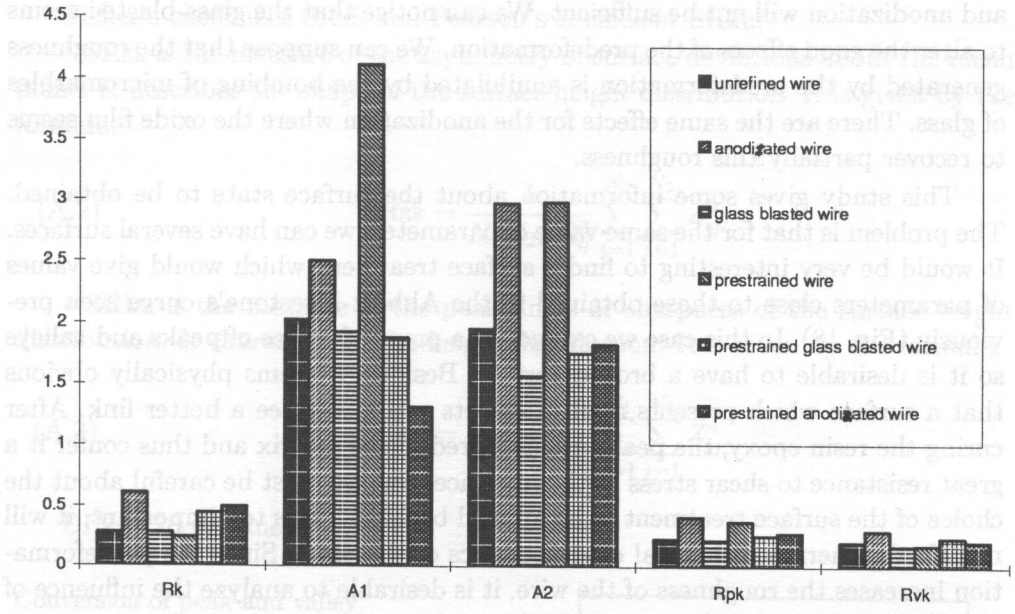


FIG. 19. Graphic representation of the parameters linked to the curve of lift.

We have the formulation

$$\text{Kp} = \frac{\text{depth of smooth}}{\text{average depth}} = \frac{\text{Rvm}}{\text{Rtm}} = 1 - \frac{\text{Rpm}}{\text{Rvm}}. \tag{4.1}$$

We give an illustration of the meaning of Kp from simulated profiles in the Appendix. In our study, we find Kp$= 0,47$ for the prestrained wire. A value of Kp $< 0,5$ means that we have a fragile configuration for the wire and a solid one for the host material, and if we consider the pullout test, it is the matrix which breaks at the interface and not the wire. We have also a solid configuration for the anodized wire but less important than the prestrained one. This parameter Kp allows us to differentiate the behaviour of the wire subjected to different surface treatments and more precisely, to confirm the results obtained during pullout tests that the prestrained wire offers the best quality of the interface.

## 5. CONCLUSIONS AND PERSPECTIVES

The whole profilometric study complies with the results obtained initially during the pullout tests. The prestrained wire seems to present the best surface state to transfer stresses to the host material. Moreover, by using the recovery stress like the actuator, the wire must necessarily be prestrained before its use,

and anodization will not be sufficient. We can notice that the glass-blasted seems to alter the good effects of the predeformation. We can suppose that the roughness generated by the predeformation is annihilated by the bombing of micromarbles of glass. There are the same effects for the anodization where the oxide film seems to recover partially this roughness.

This study gives some information about the surface state to be obtained. The problem is that for the same value of parameter, we can have several surfaces. It would be very interesting to find a surface treatment which would give values of parameters close to those obtained in the Abbott-Firestone's curve seen previously (Fig. 18). In this case we can notice a preponderance of peaks and valleys so it is desirable to have a broken surface. Besides, it seems physically obvious that a surface which presents a lot of defects will guarantee a better link. After curing the resin epoxy, the peaks are anchored in the matrix and thus confer it a great resistance to shear stress at the interface. But we must be careful about the choice of the surface treatment to be applied because if it is too important, it will modify the thermomechanical characteristics of the SMA. Since the predeformation increases the roughness of the wire, it is desirable to analyze the influence of the processing procedure (prestrain the wire first and next the surface treatment or inversely). A quantitative study of the recovery stress to transfer can be done.

## Acknowledgements

The authors would like to thank Professor J. Mignot (Laboratoire de Métrologie des Interfaces Techniques, University of Besançon) for many helpful discussions and assistance in performing the experiments.

## Appendix

We present in this paragraph the physical and mathematical meaning of the principal parameters used in this topographic study. These explanations are extracted from a report proposing a standard profilometric characterization for 3D surfaces [15].

SRa represents the arithmetic mean of the absolute values of the surface departures above and below the mean plane within the sampling area. It is given by the numerical formula

$$\text{SRa} = \frac{1}{N_1 N_2} \sum_{i=1}^{N_1} \sum_{j=1}^{N_2} |Z_{ij}| \,. \tag{A.1}$$

Fisher's coefficient SRsk and Pearson's coefficient SRku:

– SRsk is the measure of the asymmetry of surface deviations about the mean plane. It describes the shape of the surface height distribution. It is given by the formula:

$$\text{SRsk} = \frac{1}{N_1 N_2 SR_q^3} \sum_{i=1}^{N_1} \sum_{j=1}^{N_2} Z_{ij}^3. \tag{A.2}$$

– SRku is the measure of the peakedness or sharpness of the surface height distribution. It characterizes the height distribution. It is given by the formula:

$$\text{SRku} = \frac{1}{N_1 N_2 SR_q^4} \sum_{i=1}^{N_1} \sum_{j=1}^{N_2} Z_{ij}^4. \tag{A.3}$$

DIN 4776 parameters

Conversion of peak and valley areas into equivalent area triangles

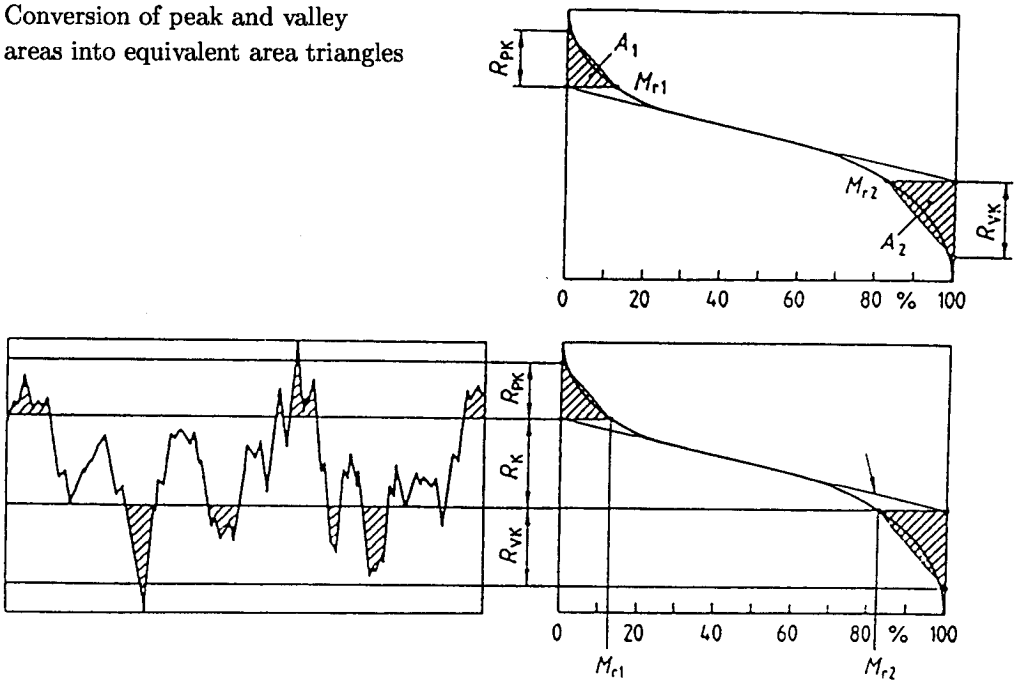


FIG. 20. The diagram of DIN 4776 parameters [15].

The parameter Rk – the core roughness depth- measures the height of the core material portion. It applies to at the region with the flattest change on the Abbott curve where the largest increase in materials exists. It is determined

graphically by plotting the tangent to the Abbott curve which passes through at least 40% of the points.

The parameter Rpk (Rvk) is called the reduced peak height (the reduced valley depth) which denotes the height of the profile peak projecting beyond the core profile (the proportion of profile valleys extending into the material below the core profile).

MR1 and MR2 represent the bearing area points.

Meaning of Kp:

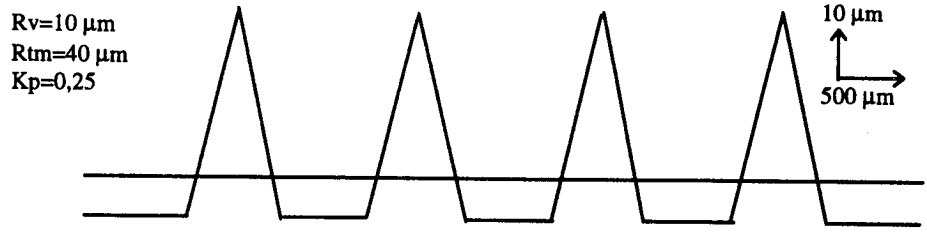


0<Kp<<0,5 : the profile has a " fragile' form : sharp ledges and wide troughs.

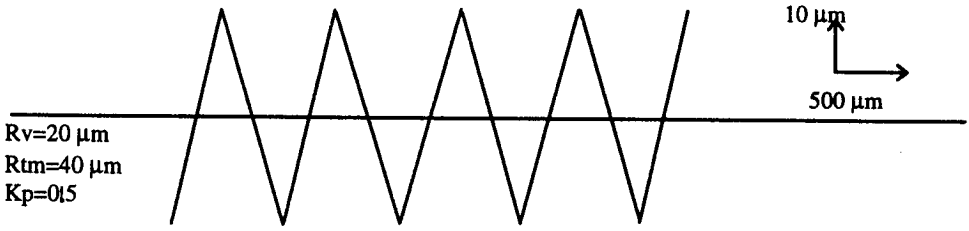


Kp=0,5 : The profile is perfectly symmetrical

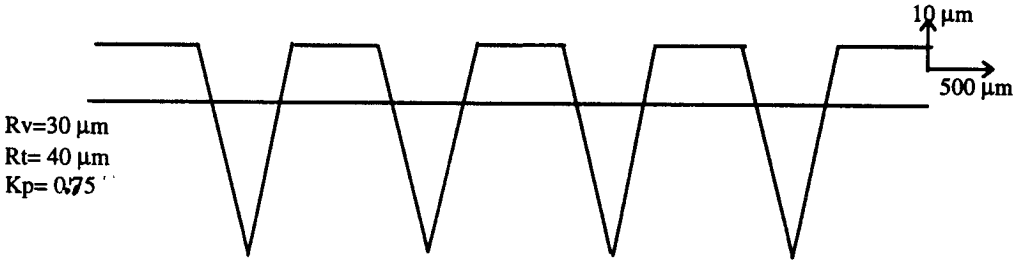


0,5<Kp<<1 : the profile has a " sturdy" form : wide ledges and narrow troughs.

FIG. 21. Meaning of Kp [16].

A1 (A2) represents the area of peaks (valleys) located above (below) the core profile and it is proportional to the number of peaks (valleys) and to their height (depth) too. The same value of these areas can correspond to a large number of peaks (valleys) of small height (depth) or conversely. They are given by the formulas

$$\text{(A.4)} \qquad \text{A1} = \frac{\text{Rpk} \cdot \text{MR1}}{2} \qquad \text{or} \qquad \text{A2} = \frac{\text{Rvk} \cdot (100 - \text{MR2})}{2}$$

## REFERENCES


1. C. LIANG, J. LIA and C. ROGERS, *Behavior of shape memory alloy reinforced composite plates*, Proceedings of 30th Structures, Structural Dynamics and Material Conference, AIAA-89-1331-CP, pp. 1504–1513, 1989.
2. A. BAZ, S. POH, J. RO, M. MUTUA and J. GILHEANY, *Active control of Nitinol-reinforced composite beam*, Intelligent Structural Systems, pp. 169–212, 1992.
3. Y. FURUYA, *Design and experimental verifications of intelligent materials using shape memory alloy*, Proceedings of the International Symposium on Microsystems, Intelligent Materials and Robots, Sendai, Japan, September 27-29, 1995.
4. M. SALVIA and J. GRANDO, *Influence des conditions déaboration sur les performances des composites hybrides adaptables*, Journées Nationales sur les Composites, no 10, 29-30-31 octobre 1996, Paris 1996, pp. 123–130, 1996.
5. J. JIA and C.A. ROGERS, *Formulation of a mechanical model for composites with embedded S.M.A. actuators*, The American Society of Mechanical Engineers, Book No H00506 pp. 203–210, 1989.
6. G. XU, D.C. LAGOUDAS, J.T. WEN, D. HUGHES, *Thermo-electro-mechanical modeling and structural response of a flexible beam with external S.M.A. actuators*, SPIE 2442, pp. 503–515, 1995.
7. K. JONNALAGADDA, G. E. KLINE and N. R. SOTTOS, *Local displacements and load transfer in shape memory alloy composites*, Theoretical and Applied Mechanics, Report NO. UILU -ENG 95-6027, 1995.
8. P. LE MOAL and D. PERREUX, *Evaluation of creep compliances of unidirectional fibre reinforced composites*, Composites, Science and Technology, pp. 469–477, 1993.
9. S. LECLERCQ and C. LEXCELLENT, *A general macroscopic description of the thermomechanical behavior shape memory alloys*, Journal of Mechanics and Physics of Solids, 44, NO. 6, pp. 953–980, 1996.
10. S. LECLERCQ, *De la modélisation thermomécanique et de l'utilisation des alliages á mémoire de forme*, Thèse de l'Université de Franche-Comté en S.P.I., juin 1995.
11. CHUN-HWAY HSUEH, *Embedded end debonding during fiber pull-out*, MaterialsScience and Engineering, A163 L1-L4, 1993.
12. J.P. FAVRE, G. DESARMOT, V. ORLIONNET and F. SAINT ANTONIN, *Techniques de fragmentation pour la mesure de l'adhésion fibre-matrice*, Journées Nationales sur les Composites NO.5 – pluralis, pp. 210–223, Paris 1986.

13. B. GRESZCZUK, *Theoretical studies of the mechanics of the fiber-matrix interface in composites*, ASTM STP 452, American Society for Testing and Material, pp. 42–58, 1969.

14. J. E. BIDAUX, J. A. E. MANSON, R. GOTTHARDT, *Active stiffening of composite materials by embedded shape-memory-alloy fibres*, Material Research Society, Symp. Proc., **459**, pp. 107–117, 1997.

15. K. J. STOUT, P.J. SULLIVAN, W.P. DONG, E. MAINSAH, N. LUO, T. MATHIA and H. ZAHOUANI, *The development methods for the characterization of roughness in 3 dimensions*, phase II report, vol. 1 and 2, 1993.

16. C. FAYOLLE, *Analyse statistique de la topographie des surfaces*, Thèse de Docteur Ingénieur, spécialité mécanique, Ecole Centrale de Lyon, mars 1983.

**LABORATOIRE DE MÉCANIQUE APPLIQUÉE R. CHALÉAT**
**UMR 6604 CNRS, UFR SCIENCES ET TECHNIQUES**
**INSTITUT DES MICROTECHNIQUES DE FRANCHE COMTÉ FR 0067**

24 rue de l'Epitaphe – 25030 Besançon cedex
Tel: (33) 03 81 66 60 09 Fax: (33) 03 81 66 67 00

E-mail: frederic.thiebaud@univ-fcomte.fr

*Received July 14, 1998.*